

A Late Pleistocene Sea Level Stack

R. M. Spratt¹ and L. E. Lisiecki¹

[1] {Department of Earth Science, University of California, Santa Barbara, United States}

Correspondence to: L. E. Lisiecki (lisiecki@geol.ucsb.edu)

Abstract

Late Pleistocene sea level has been reconstructed from ocean sediment core data using a wide variety of proxies and models. However, the accuracy of individual reconstructions is limited by measurement error, local variations in salinity and temperature, and assumptions particular to each technique. Here we present a sea level stack (average) which increases the signal-to-noise ratio of individual reconstructions. Specifically, we perform principal component analysis (PCA) on seven records from 0-430 ka and five records from 0-798 ka. The first principal component, which we use as the stack, describes ~80% of the variance in the data and is similar using either five or seven records. After scaling the stack based on Holocene and Last Glacial Maximum (LGM) sea level estimates, the stack agrees to within 5 m with isostatically adjusted coral sea level estimates for Marine Isotope Stages 5e and 11 (125 and 400 ka, respectively). Bootstrapping and random sampling yield mean uncertainty estimates of 9-12 m (1σ) for the scaled stack. Sea level change accounts for about 45% of the total orbital-band variance in benthic $\delta^{18}\text{O}$, compared to a 65% contribution during the LGM-to-Holocene transition. Additionally, the second and third principal components of our analyses reflect differences between proxy records associated with spatial variations in the $\delta^{18}\text{O}$ of seawater.

1 Introduction

Glacial-interglacial cycles of the Late Pleistocene (0-800 ka) produced sea level changes of approximately 130 meters, primarily associated with the growth and retreat of continental ice sheets in 100-ka cycles. Recent ice sheet modeling studies support the assertion of Milankovitch theory that Late Pleistocene glacial cycles are primarily driven by insolation changes associated with Earth's orbital cycles (Ganopolski and Calov, 2011; Abe-Ouchi et al. 2013). However,

1 modeling ice sheet responses over orbital timescales remains quite challenging, and the output
2 of such models should be evaluated using precise and accurate reconstructions of sea level
3 change. Thus, Late Pleistocene sea level reconstructions are important both for understanding
4 the mechanisms responsible for 100-ka glacial cycles and for quantifying the amplitude and
5 rate of ice sheet responses to climate change. Sea level estimates for warm interglacials at 125
6 and 400 ka are also of particular interest as potential analogs for future sea level rise (Kopp et
7 al., 2009; Raymo and Mitrovica, 2012; Dutton et al., 2015).

8 Nearly continuous coral elevation data have generated well-constrained sea level
9 reconstructions since the Last Glacial Maximum (LGM) at 21 ka (Clark et al., 2009; Lambeck
10 et al., 2014). However, beyond the LGM sea level estimates from corals are discontinuous and
11 have relatively large age uncertainties (e.g., Thompson and Goldstein, 2005; Medina-Elizalde,
12 2013). Several techniques have been developed to generate longer continuous sea level
13 reconstructions from marine sediment core data. Each of these techniques is subject to different
14 assumptions and regional influences. Here, we identify the common signal present in seven
15 Late Pleistocene sea level records as well as some of their differences.

16 These sediment core records convert $\delta^{18}\text{O}_c$, the oxygen isotope content of the calcite tests of
17 foraminifera, to sea level using one of several techniques. In three records, temperature proxies
18 were used to remove the temperature-dependent fractionation effect from $\delta^{18}\text{O}_c$ in order to solve
19 for the $\delta^{18}\text{O}$ of seawater ($\delta^{18}\text{O}_{sw}$). Other techniques for transforming $\delta^{18}\text{O}_c$ to sea level include
20 the polynomial regression of $\delta^{18}\text{O}_c$ to coral-based sea level estimates, hydraulic control models
21 of semi-isolated basins, and inverse models of ice volume and temperature. Each of these
22 techniques produce slightly different results for a variety of reasons. For example, $\delta^{18}\text{O}_{sw}$ varies
23 spatially due to differences in water mass salinity and deep water formation processes (Adkins
24 et al., 2002). Reconstructions also vary based on sensitivity to eustatic versus relative sea level
25 (RSL) and temporal resolution.

26 Principal component analysis (PCA) is used to identify the common sea level signal in these
27 seven records (i.e., to produce a sea level “stack”) and to evaluate differences between
28 reconstruction techniques. By combining multiple sea level records with different underlying
29 assumptions and sources of noise, the sea level stack should have a higher signal-to-noise ratio
30 than the individual sea level records used to construct it. We estimate the uncertainty of the sea
31 level stack using bootstrapping and Monte Carlo-style random sampling. For comparison, we
32 also report the standard deviation of highstand and lowstand estimates across individual records

1 and the sea level uncertainties of individual records as estimated in their original publications.
2 A probabilistic reassessment of the uncertainties in individual records is beyond the scope of
3 the current study.

4

5 **2 Sea level reconstruction techniques**

6 **2.1 Corals and other coastal sea level proxies**

7 Corals provide the most prominent Late Pleistocene sea level proxy. They can be
8 radiometrically dated and provide especially accurate sea level estimates between 0-21 ka
9 because of nearly continuous pristine coral specimens from several locations (Fairbanks, 1989;
10 Bard et al., 1990; Edwards et al., 1993; Bard et al., 1996). Dated coral sea level estimates extend
11 as far back as ~600 ka (Stein et al., 1993; Stirling et al., 1995; Medina-Elizalde, 2013; Muhs et
12 al., 2014; Andersen et al., 2008). However, coral data are increasingly discontinuous and
13 inaccurate prior to 21 ka due to difficulty finding pristine and in situ older corals (particularly
14 during sea level lowstands) and due to U-Th age uncertainties in older corals caused by isotope
15 free exchange with the surrounding environment (e.g., Thompson and Goldstein, 2005;
16 Blanchon et al., 2009; Medina-Elizalde, 2013). Interpretation of sea level from corals often
17 requires a correction for rates of continental uplift, which may not be known precisely
18 (Creveling et al., 2015). Glacial isostatic adjustment (GIA) and species habitat depth (up to 6
19 m below sea level) may also affect sea level estimates (Raymo and Mitrovica, 2012; Medina-
20 Elizalde, 2013). Wave destruction and climate variations also alter coral growth patterns and
21 may affect the height of colonies relative to sea level (Blanchon et al., 2009; Medina-Elizalde,
22 2013).

23 Organic proxies such as peat bogs and shell beds can also be used as sea level proxies and can
24 be radiometrically dated (e.g., Horton, 2006). Geological formations indicating sea level such
25 as abandoned beaches and sea cliffs can also be used as sea level proxies (Hanebuth et al., 2000;
26 Boak and Turner, 2005; Bowen, 2010).

27 Corals and other coastal proxies are indicators of relative (local) sea level and, thus, are affected
28 by in situ glacio isostatic effects, ocean siphoning processes, and other local effects of sea level
29 rise and fall. However, their wide spatial distribution, particularly corals in tropical regions,

1 allows for modeling of glacioisostatic adjustments (GIA) to create a global estimate of mean
2 sea level change (e.g., Kopp et al., 2009; Lambeck et al., 2014; Dutton and Lambeck, 2012;
3 Hay et al., 2014). GIA models constrained by these coastal indicators provide robust sea level
4 change estimates of -130 to -134 m for the LGM (Clark et al., 2009; Lambeck et al., 2014). A
5 compilation of dozens of corals and other sea level indicators also provide relatively well-
6 constrained estimate of 8.7 ± 0.7 m for peak global mean sea level at the last interglacial (Kopp
7 et al., 2009). Estimates from multiple studies using different data are all in relatively good
8 agreement yielding a consensus estimate of 6 to 9 m above modern (Dutton et al., 2015).
9 Additionally, sea level during last interglacial likely experienced several meters of millennial-
10 scale variability (Kopp et al., 2013; Govin et al., 2012). Uncertainties increase for older
11 interglacials. GIA-corrected coastal sea level proxies for Marine Isotope Stage (MIS) 11 at ~400
12 ka suggest a global mean sea level of 6-13 m above modern (Raymo and Mitrovica, 2012).

13 **2.1 Seawater $\delta^{18}\text{O}$**

14 Global ice volume is a main control on the global mean of $\delta^{18}\text{O}$ in seawater ($\delta^{18}\text{O}_{\text{sw}}$), with global
15 mean $\delta^{18}\text{O}_{\text{sw}}$ estimated to decrease by 0.008‰ to 0.01‰ per meter of sea level rise (Adkins et
16 al., 2002; Elderfield 2012; Shakun et al., 2015). However, $\delta^{18}\text{O}_{\text{sw}}$ also varies spatially based on
17 patterns of evaporation and precipitation and deep water formation processes. The $\delta^{18}\text{O}$ of
18 calcite ($\delta^{18}\text{O}_{\text{c}}$) is affected both by the $\delta^{18}\text{O}_{\text{sw}}$ and temperature. In the absence of any post-
19 depositional alteration, subtracting the temperature-dependent fractionation effect from $\delta^{18}\text{O}_{\text{c}}$
20 (Shackleton, 1974) should yield a good estimate of the $\delta^{18}\text{O}_{\text{sw}}$ in which the calcite formed.
21 Pioneering studies for estimating time series of $\delta^{18}\text{O}_{\text{sw}}$ using independent measures of
22 temperature include Dwyer et al. (1995), Martin et al. (2002), and Lea et al. (2002). Dwyer et
23 al. (1995) used ostracod Mg/Ca ratios to determine temperature whereas Martin et al (2002)
24 and Lea et al (2002) used benthic and planktonic foraminifera, respectively. The $\delta^{18}\text{O}_{\text{c}}$ of
25 benthic foraminifera reflects the temperature and $\delta^{18}\text{O}_{\text{sw}}$ of deep water, while the $\delta^{18}\text{O}_{\text{c}}$ of
26 planktonic foraminifera is affected by sea surface temperature (SST) and the $\delta^{18}\text{O}_{\text{sw}}$ of near-
27 surface water.

28 **2.2 Benthic $\delta^{18}\text{O}_{\text{sw}}$**

29 Our analysis includes two benthic $\delta^{18}\text{O}_{\text{sw}}$ records from the North Atlantic and South Pacific,
30 which use the Mg/Ca ratio of benthic foraminifera as a temperature proxy. The South Pacific
31 benthic $\delta^{18}\text{O}_{\text{sw}}$ record (Elderfield et al., 2012) from Ocean Drilling Program (ODP) site 1123

1 (171 W, 41 S, 3290 m) reflects the properties of Lower Circumpolar Deep Water, which is a
2 mix of Antarctic Bottom Water (AABW) and North Atlantic Deep Water (NADW). Mg/Ca
3 ratios and $\delta^{18}\text{O}_c$ were determined from separate samples of the same species of *Uvigerina*,
4 which is considered fairly insensitive to the deep water carbonate saturation state (Elderfield et
5 al., 2012). Elderfield et al. (2012) interpolate their data to 1 ka spacing, perform a 5-ka Gaussian
6 smoothing, and convert from $\delta^{18}\text{O}_{\text{sw}}$ to sea level using a factor of 0.01‰m^{-1} . Elderfield et al.
7 (2012) report measurement uncertainties for temperature and $\delta^{18}\text{O}_c$ generate a $\delta^{18}\text{O}_{\text{sw}}$
8 uncertainty of $\pm 0.2\text{‰}$, corresponding to bottom water temperature range of $\pm 1^\circ\text{C}$ or about 22
9 m of sea level.

10 The North Atlantic $\delta^{18}\text{O}_{\text{sw}}$ reconstruction is from Deep Sea Drilling Program (DSDP) site 607
11 (32 W, 41 N, 3427 m) and nearby piston core Chain 82-24-23PC (Sosdian and Rosenthal,
12 2009). These sites are bathed by NADW today but were likely influenced by AABW during
13 glacial maxima (Raymo et al., 1990). Mg/Ca was measured using two benthic foraminiferal
14 species, *Cibicidoides wuellerstorfi* and *Oridorsalis umbonatus*, which may be affected by
15 changes in carbonate ion saturation state, particularly when deep water temperature drops below
16 3°C (Sosdian and Rosenthal, 2009). The $\delta^{18}\text{O}_c$ data come from a combination of *Cibicidoides*
17 and *Uvigerina* species. Sea level was estimated from benthic $\delta^{18}\text{O}_{\text{sw}}$ using a conversion of
18 0.01‰m^{-1} and then taking a 3-point running mean. Combining the uncertainties for temperature
19 ($\pm 1.1^\circ\text{C}$) and $\delta^{18}\text{O}_c$ ($\pm 0.2\text{‰}$) reported by Sosdian and Rosenthal (2009) yields a sea level
20 uncertainty of approximately ± 20 m (one standard error) for the 3-point running mean.

21 **2.3 Planktonic $\delta^{18}\text{O}_{\text{sw}}$**

22 A 49-core global stack uses the $\delta^{18}\text{O}_c$ from planktonic foraminifera paired with SST proxies
23 from the same core. The planktonic species in this reconstruction were: *G. ruber*, *G. bulloides*,
24 *G. inflata*, *G. sacculifer*, *N. dutretriei*, and *N. pachyderma*. Forty-four records span the most
25 recent glacial cycle, and seven records extend back to 798 ka. Thirty-four records use Mg/Ca
26 temperature estimates, and fifteen use the alkenone U^k_{37} temperature proxy. Because U^k_{37}
27 measurements derive from coccolithophore rather than foraminifera, there is some chance the
28 temperature measured may differ slightly from that affecting $\delta^{18}\text{O}_c$ (Schiebel et al. 2004).
29 However, Shakun et al. (2015) observed no significant differences in $\delta^{18}\text{O}_{\text{sw}}$ estimated from the
30 two SST proxies. An additional concern is that the surface ocean is affected by greater
31 hydrologic variability and characterizes a smaller ocean volume than the deep ocean. Thus,
32 planktonic $\delta^{18}\text{O}_{\text{sw}}$ may differ more from ice volume changes than benthic data. However, these

1 potential disadvantages of using planktonic records may be largely compensated by the use of
2 a global planktonic stack.

3 The first principal component (stack) of the planktonic records spanning the last glacial cycle
4 represents 71% of the variance in the records (n=44), suggesting a strong common signal in
5 planktonic $\delta^{18}\text{O}_{\text{sw}}$. However, the 800-ka planktonic $\delta^{18}\text{O}_{\text{sw}}$ stack appears to contain linear trends
6 that differ from other sea level estimates. Therefore, Shakun et al. (2015) corrected their sea
7 level estimate by detrending planktonic $\delta^{18}\text{O}_{\text{sw}}$ based on differences between planktonic and
8 benthic $\delta^{18}\text{O}_{\text{c}}$. Standard errors reported by Shakun et al. (2015) for the $\delta^{18}\text{O}_{\text{sw}}$ stack increase
9 from 0.05‰ for the last glacial cycle to 0.12‰ at 800 ka due to the reduction in the number of
10 records. The equivalent sea level uncertainties are ± 6 m and ± 18 m (1σ), respectively. All data
11 were interpolated to even 3 ka time intervals.

12 **2.4 Benthic $\delta^{18}\text{O}_{\text{c}}$ - coral regression**

13 The sea level reconstruction of Waelbroeck et al. (2002) was developed by fitting polynomial
14 regressions between benthic $\delta^{18}\text{O}_{\text{c}}$ from North Atlantic cores NA 87-22/25 (55 N, 15 W, 2161
15 and 2320 m) and equatorial Pacific core V19-30 (3 S, 83 W, 3091 m) to sea level estimates for
16 the last glacial cycle, primarily from corals. Quadratic polynomials were fit during times of ice
17 sheet growth and during the glacial termination in the North Atlantic whereas a linear regression
18 was fit to the Pacific glacial termination. A composite sea level curve was created from the
19 most reliable sections of several cores, primarily from the Pacific. Waelbroeck et al. (2002)
20 interpolated the composite time series to an even 1.5 ka time window and estimated the
21 uncertainty associated with this technique to be ± 13 m of sea level. Transfer functions between
22 benthic $\delta^{18}\text{O}_{\text{c}}$ and coral sea level estimates have also been estimated at lower resolution and
23 applied to 10 different benthic $\delta^{18}\text{O}$ records spanning 0-5 Ma (Siddall et al., 2010; Bates et al.,
24 2014).

25 **2.5 Inverse ice volume model**

26 The inverse model of Bintanja et al. (2005) is based on the concept that Northern Hemisphere
27 (NH) subpolar surface air temperature plays a key role in determining both ice sheet size and
28 deepwater temperature, which are the two dominant factors affecting benthic $\delta^{18}\text{O}_{\text{c}}$. A three-
29 dimensional thermomechanical ice sheet model simulates ice sheet $\delta^{18}\text{O}$ content, height, and
30 volume for NH ice sheets (excluding Greenland) as forced by subpolar air temperature, orbital

1 insolation, and the modern spatial distributions of temperature and precipitation. Antarctic and
2 Greenland ice sheets are assumed to account for 5% of ocean isotopic change and 15% of sea
3 level change. Deep water temperature is assumed to scale linearly with the 3-ka mean air
4 temperature. At each time step air temperature is adjusted to maximize agreement between
5 predicted $\delta^{18}\text{O}_c$ and the observed value 0.1 ka later in a benthic $\delta^{18}\text{O}_c$ stack (Lisiecki and
6 Raymo, 2005). The model solves for ice volume, temperature, and sea level changes since 1070
7 ka in 0.1 ka time steps; however, the $\delta^{18}\text{O}_c$ stack used to constrain the model has a resolution
8 of 1-1.5 ka. Bintanja et al. (2005) report the uncertainty of their sea level model to be
9 approximately ± 12 m (1σ)

10 **2.6 Hydraulic control models of semi-isolated basins**

11 Two sea level reconstructions use hydraulic control models to relate planktonic $\delta^{18}\text{O}_c$ from the
12 Red Sea and Mediterranean Sea to relative sea level. In these semi-isolated basins, $\delta^{18}\text{O}_{sw}$ is
13 strongly affected by evaporation and exchange with the open ocean as affected by relative sea
14 level at the basin's sill.

15 Red Sea RSL (Rohling et al., 2009) from 0-520 ka is estimated using the $\delta^{18}\text{O}_c$ of planktonic
16 foraminifera from the central Red Sea (GeoTü-KL09). Because extremely saline conditions
17 killed foraminifera during MIS 2 and MIS 12, $\delta^{18}\text{O}_c$ data for these time intervals were estimated
18 by transforming bulk sediment values. Sea level is estimated using a physical circulation model
19 for the Red Sea combined with an oxygen isotope model (Siddall et al., 2004). The physical
20 circulation model simulates exchange flow through the Bab-el-Mondab strait which depends
21 strongly on sea level. The current sill depth is 137 m, and its estimated uplift rate is 0.2 m ka^{-1} .
22 The isotope model assumes steady state with exchange through the sill and
23 evaporation/precipitation. Assumptions of the isotope model include: (1) modern evaporation
24 rates and humidity, (2) open ocean $\delta^{18}\text{O}_{sw}$ scales as 0.01‰m^{-1} , and (3) SST scales linearly with
25 sea level. A 5° C change in SST between Holocene and LGM is used to optimize the model's
26 LGM sea level estimate. Steady state model solutions for different sea level estimates are used
27 to develop a conversion between $\delta^{18}\text{O}_c$ and sea level, which is approximated as a fifth-order
28 polynomial. Rohling et al. (2009) performed sensitivity tests using plausible ranges of climatic
29 values to produce a $2\text{-}\sigma$ uncertainty estimate of ± 12 m.

30 A Mediterranean RSL record (Rohling et al., 2014) is derived from a hydraulic model of flow
31 through the Strait of Gibraltar (Bryden and Kinder, 1991) combined with evaporation and

1 oxygen isotope fractionation equations for the Mediterranean (Siddall et al., 2004). Runoff and
2 precipitation are parameterized based on present-day observations, humidity is assumed
3 constant, and temperature is assumed to covary with sea level. The $\delta^{18}\text{O}_{\text{sw}}$ of Atlantic inflow is
4 scaled using 0.009‰m^{-1} , and net heat flow through the sill is assumed to be zero. The combined
5 models yield a converter between $\delta^{18}\text{O}_{\text{c}}$ and sea level, which is approximated as a polynomial.
6 This polynomial conversion is applied to an eastern Mediterranean planktonic $\delta^{18}\text{O}_{\text{c}}$ stack
7 (Wang et al., 2010) after identification and removal of sapropel layers. Model uncertainty is
8 evaluated using random parameter variations, which yield 95% confidence intervals of ± 20 m
9 for individual $\delta^{18}\text{O}_{\text{c}}$ values. By performing a probabilistic assessment of the final sea level
10 reconstruction with 1-ka time steps, Rohling et al. (2014) estimate that these uncertainties are
11 reduced to ± 6.3 m. Additionally, the authors propose that RSL at this location is linearly
12 proportional to eustatic sea level.

13 **3 Methods**

14 **3.1 Record inclusion criteria**

15 The criteria for record inclusion in our stack were availability, a temporal resolution of at least
16 5 ka, and a length of at least 430 ka. The five records which extended to 798 ka were also
17 included in a longer stack. Some available records were too short for inclusion (e.g., Dwyer et
18 al., 1995; Martin et al, 2002; Lea et al., 2002). The record of Siddall et al (2010) was not
19 included because it was based on the same technique as Waelbroeck et al (2002) but with
20 lower resolution. Bates et al (2014) extended this technique to many benthic $\delta^{18}\text{O}$ records but
21 advocated against placing them all on a common age model; therefore, we include a summary
22 of that study's lowstand and highstand estimates in Table 2 rather than aligning them for
23 inclusion in the stack.

24 **3.2 Age models**

25 To create an average (or stack) of sea level records, all of the time series must be placed
26 on a common age model (Fig. 1). Here we use the age model of the orbitally tuned "LR04"
27 benthic $\delta^{18}\text{O}_{\text{c}}$ stack (Lisiecki and Raymo, 2005), which has an uncertainty of 4 ka in the Late
28 Pleistocene. An age model for the Red Sea reconstruction based on correlation to speleothems
29 is generally similar to LR04 with smaller age uncertainty but only extends to 500 ka (Grant et
30 al., 2014) and, thus, does not provide an age framework for the entire 798 ka stack. Due to age

1 model uncertainty, our interpretation focuses on the amplitude of sea level variability rather
2 than its precise timing.

3 We do not assume that sea level varies synchronously with benthic $\delta^{18}\text{O}_c$. Age models
4 for three of the reconstructions are based on aligning individual $\delta^{18}\text{O}_c$ records to the LR04 $\delta^{18}\text{O}_c$
5 stack, and one reconstruction (Bintanja et al., 2005) was derived directly from the LR04 stack.
6 The other three sea level reconstructions were dated by aligning their sea level estimates to a
7 preliminary stack of the four sea level records that were dated using $\delta^{18}\text{O}_c$ alignments.
8 Alignments were performed using the Match graphic correlation software package (Lisiecki
9 and Lisiecki, 2002).

10 The three records which use $\delta^{18}\text{O}_c$ alignments to the LR04 stack are Sites 607, 1123,
11 and the planktonic $\delta^{18}\text{O}_{sw}$ stack. For Site 607 we perform our own alignment of benthic $\delta^{18}\text{O}_c$
12 to the LR04 stack, whereas for the other two we use the same age models published by
13 Elderfield et al. (2012) and Shakun et al (2015). One potential concern about aligning benthic
14 $\delta^{18}\text{O}_c$ records is that the timing of benthic $\delta^{18}\text{O}_c$ change at different sites may differ by as much
15 as 4 kyr during glacial terminations (Skinner and Shackleton, 2005; Lisiecki and Raymo, 2009;
16 Stern and Lisiecki, 2014). The potential effects of lags in benthic $\delta^{18}\text{O}_c$ are evaluated using
17 bootstrap uncertainty analysis (Section 4.2).

18 For three reconstructions (Waelbroeck et al., 2002; Rohling et al., 2009, 2014) we
19 aligned the individual sea level records with a preliminary sea level stack based on the other
20 four sea level records on the LR04 age model. This was necessary because the local $\delta^{18}\text{O}_c$
21 signals in semi-isolated basins (Rohling et al., 2009; 2014) differ substantially from global
22 mean benthic $\delta^{18}\text{O}_c$. In the coral-regression reconstruction, Waelbroeck et al. (2002) pasted
23 together portions of individual cores to form a preferred global composite. Although each core
24 has benthic $\delta^{18}\text{O}_c$ data, generating new age estimates for these cores could alter their $\delta^{18}\text{O}_c$
25 regression functions or create gaps or inconsistencies in the composite. The procedure of
26 aligning these three sea level records (Waelbroeck et al, 2002; Rohling et al., 2009, 2014) to a
27 preliminary sea level stack should be approximately as accurate as the $\delta^{18}\text{O}_c$ alignments.
28 However, the direct sea level alignments do have a slightly greater potential to align noise or
29 local sea level variability.

30 After age models were adjusted, five of the records ended within the Holocene. Therefore, we
31 appended a value of 0 m (i.e., present day sea level) at 0 ka. In the two records which did end

1 at 0 ka, modern sea level estimates were slightly below zero: -1.5 m (Bintanja, 2005) and -1.3
2 m (Rohling et al., 2014).

3 **3.3 Principal component analysis**

4 Principal Component Analysis (PCA) is commonly used to create stacks of paleoclimate data
5 (e.g., Huybers and Wunsch, 2004; Clark et al, 2012; Gibbons et al, 2014) and to quantify the
6 common signal contained in core data. Synthesis is valuable because each record has its own
7 assumptions and errors. If these records are all well-constrained measures of sea level, then
8 PCA will reveal their respective levels of agreement or discrepancy. Additionally, PCA does
9 not require the assumption that each sea level record represents an independent measure of
10 common signal. In contrast, a sea level estimate based on the unweighted mean of records
11 would imply that uncertainties are uncorrelated across individual reconstructions. While all
12 records contain a strong ice volume signal, some of the non-ice volume signal are expected to
13 correlate with one another. For example, as the $\delta^{18}\text{O}$ of ice sheet changes as it melts or freezes,
14 the conversion from the $\delta^{18}\text{O}_{\text{sw}}$ to ice volume will be systematically biased, whereas changes in
15 the hydrological cycle may induce changes in the spatial variability of $\delta^{18}\text{O}_{\text{sw}}$ at different
16 locations in the ocean.

17 We include both relative and eustatic sea level estimates in the analysis because PCA should
18 identify the common variance that dominates both relative and eustatic sea level records. Three
19 records are proxies for relative sea level at their respective locations: the strait of Gibraltar
20 (Rohling et al., 2014), the Bab el Mondab strait (Rohling et al., 2009), and tropical coral terraces
21 (Waelbroeck et al., 2002). The inverse model generates eustatic sea level from a modeled ice
22 volume estimate (Bintanja et al., 2005), and the three $\delta^{18}\text{O}_{\text{sw}}$ records (Elderfield et al., 2012;
23 Sosdian and Rosenthal, 2009; Shakun et al., 2015) were scaled to eustatic sea level. However,
24 for the planktonic stack we use the $\delta^{18}\text{O}_{\text{sw}}$ record rather than the eustatic sea level conversion
25 because the sea level conversion involved detrending to make planktonic $\delta^{18}\text{O}_{\text{c}}$ values agree
26 with benthic $\delta^{18}\text{O}_{\text{c}}$. Because PCA is designed to identify the common variance between the sea
27 level proxies, it is preferable to keep the planktonic and benthic $\delta^{18}\text{O}_{\text{sw}}$ records independent of
28 one another.

29 In the Mediterranean RSL record we removed putative sapropel layers at 434-452 ka, 543-558
30 ka, and 630-663 ka as visually identified by Rohling et al. (2014). Because interpolating
31 linearly across these gaps (Fig. 1) would bias sea level estimates towards higher lowstands for

1 the glacial maxima occurring during these sapropel layers, we assumed that sea level remained
2 constant at its pre-sapropel (glacial) level and then immediately jumped to the higher sea level
3 values observed the ends of the sapropel layers (midway through the glacial terminations).
4 Although this solution is not ideal, we must assume some sea level value at these times in order
5 to include this record in the PCA.

6 Before PCA all seven records were interpolated to an even 1-ka time step. Then, to ensure equal
7 weighting for each record in the PCA, each time series was normalized to a mean of zero and a
8 standard deviation of one within each of the two time windows (0-430 ka and 0-798 ka). PCA
9 was performed on seven records from 0-430 ka and five records from 0-798 ka (Fig. 2). Because
10 PC1 produces similar loadings for each record (Table 1), the PC1 scores approximate the
11 average of all records for each point in time, which we refer to as a sea level stack.

12 We scaled the short and long stacks to eustatic sea level using an LGM value of -130 m at 24
13 ka based on a GIA-corrected coral compilation (Clark et al., 2009) and a Holocene value of 0
14 m at 5 ka. We scale the Holocene at 5 ka because eustatic sea level has been essentially constant
15 for the past 5 ka (Clark et al., 2009), whereas the sea level stacks display a trend throughout the
16 Holocene perhaps due to bioturbation in the sediment cores. Scaling the sea level stack based
17 on the mid-Holocene (rather than 0 ka) should more accurately correct for the effects of
18 bioturbation on previous interglacials because those highstand values have been subjected to
19 mixing from both above and below. Finally, a composite sea level stack was created by joining
20 the 0-430 ka stack with the 431-798 ka portion of the long stack after each was scaled to sea
21 level. Because the two scaled sea level stacks produce similar values for 0-430 ka (Fig. 2), no
22 correction was needed to combine the records.

23 **4 Uncertainty analysis**

24 Because each of the records in the PCA is a sea level proxy and PC1 describes the majority of
25 variance in the records, PC1 should represent the underlying common eustatic sea level signal
26 in all proxies. PC1 describes 82% of the variance in the seven records from 0-430 ka and 76%
27 of proxy variance from 0-798 ka. Where the two time windows overlap (Figure 2), the scaled
28 sea level stacks have a root mean square error of only 3.4 m, thereby suggesting that the long
29 stack is nearly as accurate as the short stack although it contains two fewer records. We assess
30 the uncertainty of the scaled PC1 using multiple techniques: comparison with highstand and
31 lowstand estimates from individual records (Section 4.1), comparison with the unweighted

1 mean of all records (Section 4.1), and using bootstrapping and Monte Carlo-style random
2 sampling (Section 4.2).

3 **4.1 Mean sea level estimates**

4 To test the effectiveness of using the scaled PC1 as a record of mean sea level, we compared
5 our stack with highstand and lowstand values identified from individual records and with coral-
6 based estimates where available (Tables 2 and 3). We picked the relevant highstand or lowstand
7 for each individual record by choosing the peak that lies within the age range of each Marine
8 Isotope Stage (MIS) as identified in the sea level stack. Highstand or lowstand peaks which
9 occurred outside of the age range of each particular glacial or interglacial stage were not used
10 (e.g., extreme values at ~250 ka from ODP Sites 1123 and 607).

11 Highstand sea level estimates vary widely between individual records with standard deviations
12 of 11-26 m for each isotopic stage (Table 3). For example, individual estimates for MIS 11 at
13 ~400 ka vary between -5 to 57 m above modern, with a mean of 18 m and a standard deviation
14 of 25 m. MIS 5e (119-126 ka) estimates range from -4 to 28 m above modern with a mean of 7
15 m and a standard deviation of 12 m. Generally, the highstand means have slightly greater
16 amplitudes than our scaled stack; for example, the scaled stack estimates are 18 m and 7 m for
17 MIS 11 and MIS 5e, respectively. On the other hand, the mean of individual lowstands for the
18 LGM (-123 m) underestimates eustatic sea level change, which is estimated to be -130 to -134
19 m (Clark et al, 2009; Lambeck et al., 2014).

20 The means of the individually picked highstands may be biased by the additive effects of noise.
21 Conversely, the stack may underestimate sea level highstands if the individual age models are
22 not properly aligned. The most definitive sea level estimates come from GIA-corrected coral
23 compilations, which yield highstand estimates of 6-13 m above modern for MIS 11 (Raymo
24 and Mitrovica, 2012) and 8-9.4 m for MIS 5e (Kopp et al., 2009). These values suggest that the
25 stack may be more accurate for MIS 11 than MIS 5e, potentially because age model uncertainty
26 would have less effect on the longer MIS 11 highstand. In contrast, MIS 5e may have consisted
27 of two highstands each lasting only ~2 ka separated by several thousand years with sea level at
28 or below modern (Kopp et al., 2013). Thus, the stack's highstand estimates likely fail to capture
29 short-term sea level fluctuations but rather reflect mean sea level during each interglacial.

30 To further test the sensitivity of our method, we compared the scaled PC1 with the unweighted
31 mean of the seven interpolated sea level records (Figure 2b). The unweighted-mean stack

1 incorporates the same data as scaled PC1 except that it excludes Mediterranean estimates from
2 sapropel intervals and uses the detrended sea level estimates from Shakun et al. (2015) instead
3 of the raw $\delta^{18}\text{O}_{\text{sw}}$ data. The unweighted stack closely resembles PC1 because the loadings of
4 PC1 are very similar for all seven records (Table 1). However, the unweighted stack
5 underestimates LGM sea level, possibly because some records (e.g., Rohling et al, 2009) may
6 contain brief gaps at the glacial maximum. Thus, we prefer to scale PC1 to agree with well-
7 constrained LGM sea level estimates. The scaled PC1 is in better agreement with the glacial
8 sea level estimates of the unweighted five-record stack from 430-798 ka.

9

10 **4.2 Bootstrapping and random sampling**

11 We estimate uncertainty in the stack using a bootstrap technique instead of using the published
12 uncertainty estimates for each sea level reconstruction, which are based on different
13 assumptions and techniques and do not necessarily include all sources of uncertainty (e.g.,
14 uncertainty in benthic $\delta^{18}\text{O}_{\text{c}}$ alignments). We ran 1000 bootstrap iterations while also
15 performing random sampling to account for several of the uncertainties associated with our
16 method. Before each iteration of the bootstrapped PCA, we simulate the effects of uncertainty
17 associated with our age model alignments by applying an independent age shift of -2, -1, 0, +1,
18 or +2 ka to each component record, with each potential value selected with equal probability.
19 After performing each iteration of the PCA, we use random sampling to evaluate the effects of
20 uncertainty associated with scaling PC1 to Holocene and LGM sea level. The particular
21 Holocene point scaled to 0 m is randomly sampled from 0 – 6 ka with uniform distribution. The
22 LGM age is identified as the minimum sea level estimate between 19-34 ka, and the sea level
23 to which it is scaled is sampled with a normal distribution centered at 132 m with a standard
24 deviation of 2 m. The bootstrap results for the scaled PC1 yield a mean standard deviation of
25 9.4 m with seven records (0-430 ka) and 12 m with five records (0-798 ka). Additionally, the
26 inclusion of age uncertainty in the bootstrap analysis has the effect of systematically smoothing
27 the record. Because many of the individual reconstructions are of low resolution relative to brief
28 interglacial highstands such as MIS 5e and 7e, the bootstrapped median is biased towards
29 underestimating these highstands (Figure 2c). Therefore, in Table 3 we additionally describe
30 the 95% confidence interval for sea level maxima and minima in the bootstrapped samples.

1 **5 The sea level contribution to benthic $\delta^{18}\text{O}_c$**

2 The sea level stack and the LR04 benthic $\delta^{18}\text{O}_c$ stack are strongly correlated ($r = -0.90$).
3 However, because $\delta^{18}\text{O}_c$ contains both an ice volume and temperature component, the $\delta^{18}\text{O}_c$
4 record has a greater amplitude than the ice volume-driven $\delta^{18}\text{O}_{sw}$ record. The spectral variance
5 of $\delta^{18}\text{O}_{sw}$ and $\delta^{18}\text{O}_c$ in each orbital band can be used to determine the relative contributions of
6 sea level and temperature variability in $\delta^{18}\text{O}_c$. For this comparison, we convert the sea level
7 stack to $\delta^{18}\text{O}_{sw}$ using 0.009‰ m^{-1} .

8 Although some studies have used 0.01‰m^{-1} (e.g., Sosdian et al., 2009; Elderfield et al., 2012;
9 Rohling et al., 2009), this conversion factor is likely too high for global mean $\delta^{18}\text{O}_{sw}$ change at
10 the LGM. Several lines of evidence suggest an LGM $\delta^{18}\text{O}_{sw}$ change of 1–1.1‰ (Duplessy et
11 al., 2002; Adkins et al., 2002; Elderfield et al., 2012; Shakun et al., 2015), while LGM sea level
12 was likely 125-134 m below modern (Clark et al., 2009; Lambeck et al., 2014; Rohling et al,
13 2014). These estimates suggest a conversion factor between 0.008-0.009‰m⁻¹. A conversion
14 of 0.008‰m^{-1} would be consistent with a $\delta^{18}\text{O}_{ice}$ of -32‰ (Elderfield et al., 2012), similar to
15 estimates for the Laurentide and Eurasian ice sheets (Duplessy et al., 2002; Bintanja et al., 2005;
16 Elderfield et al., 2012). Therefore, 0.009‰m^{-1} may be more appropriate when also considering
17 changes in Greenland and Antarctic ice. However, the conversion factor between sea level and
18 mean $\delta^{18}\text{O}_{sw}$ also likely varies through time as a result of changes in the mean isotopic content
19 of each ice sheet (Bintanja et al, 2005) and their relative sizes.

20 Spectral analysis shows strong 100-ka and 41-ka peaks in both the LR04 benthic $\delta^{18}\text{O}_c$ stack
21 and the sea level stack (Figure 3). When converted to $\delta^{18}\text{O}_{sw}$, the sea level stack contains 47%
22 as much 100-ka power (0.009-0.013 ka⁻¹ frequency band) as benthic $\delta^{18}\text{O}_c$ as benthic $\delta^{18}\text{O}_c$ and
23 37% as much 41-ka power (0.024-0.026 ka⁻¹). The bootstrapped PC1 samples described in
24 Section 4.2 are used to estimate 95% confidence intervals (CI) of 31-65% and 22-54% for the
25 relative power of $\delta^{18}\text{O}_{sw}$ in the 100-ka and 41-ka bands, respectively. Considering all
26 frequencies less than 0.1 ka⁻¹, $\delta^{18}\text{O}_{sw}$ explains 44% (95% CI = 33-57%) of the variance in $\delta^{18}\text{O}_c$.
27 Therefore, we estimate that on average about 45% of the glacial cycle variance in benthic $\delta^{18}\text{O}_c$
28 derives from ice volume change and 55% from deep sea temperature change.

29 This ~45% ice volume contribution to benthic $\delta^{18}\text{O}_c$ is smaller than the contribution estimated
30 across the LGM to Holocene transition. An LGM sea level change of 130 m (Clark et al., 2009)
31 should shift mean $\delta^{18}\text{O}_{sw}$ by 1.17‰, whereas benthic $\delta^{18}\text{O}_c$ changed by 1.79‰ (Lisiecki and

1 Raymo, 2005), suggesting that 65% of the LGM $\delta^{18}\text{O}_c$ change was driven by ice volume. Many
2 other studies have similarly found that the ice volume ($\delta^{18}\text{O}_{sw}$) contribution to $\delta^{18}\text{O}_c$ is greatest
3 during glacial maxima (Bintanja et al, 2005; Elderfield et al, 2012; Rohling et al., 2014; Shakun
4 et al, 2015). Additionally, the $\delta^{18}\text{O}_{sw}$ contribution varies by location, ranging from 0.7‰ to
5 1.37‰ based on glacial pore water reconstructions (Adkins et al., 2002). The wide variability
6 in $\delta^{18}\text{O}_{sw}$ between sites suggests that changes in deep water formation processes (e.g.,
7 evaporation versus brine rejection) greatly affect the $\delta^{18}\text{O}_{sw}$ signal regionally or locally.
8 Therefore, the $\delta^{18}\text{O}_{sw}$ at a single site may differ considerably from eustatic sea level.

9 **6 Converting from benthic $\delta^{18}\text{O}_c$ and sea level**

10 Many studies have used benthic $\delta^{18}\text{O}_c$ as a proxy for ice volume based on the argument that
11 temperature and ice volume should be highly correlated through time (e.g., Imbrie and Imbrie,
12 1980; Abe-Ouchi et al., 2013). However, calculations based on the sea level stack spectral
13 power and LGM-to-Holocene change, suggest that ice volume change accounts for only 45-
14 65% of benthic $\delta^{18}\text{O}_c$ glacial cyclicity. Additionally, over the course of a glacial cycle the
15 relative contributions of ice volume and temperature change dramatically, with temperature
16 change preceding ice volume change (Bintanja et al., 2005; Elderfield et al., 2012; Shakun et
17 al., 2015). Despite these complications the LR04 benthic $\delta^{18}\text{O}_c$ stack is strongly correlated with
18 the sea level stack ($r = -0.9$). Here we explore more closely the functional relationship between
19 benthic $\delta^{18}\text{O}_c$ and sea level as inspired by Waelbroeck et al (2002).

20 Waelbroeck et al. (2002) solved for regression functions between several benthic $\delta^{18}\text{O}_c$ records
21 and coral elevation data over the last glacial cycle and found different functional forms for
22 glaciation versus deglaciation and for the North Atlantic versus equatorial Pacific $\delta^{18}\text{O}_c$. Here
23 we compare the LR04 global benthic stack with the sea level stack from 0-798 ka. One
24 advantage of this comparison is that both records use the same age model. We evaluate whether
25 a single regression can be used for the Late Pleistocene and identify a potential change in the
26 relationship between benthic $\delta^{18}\text{O}_c$ and sea level at ~400 ka.

27 One difference between the two stacks is that the sea level stack is smoother (Fig. 2), likely
28 because some of the sea level records are low resolution and all records were interpolated to 1
29 ka spacing for PCA. Smoothing the LR04 stack using a 7-ka running mean improves the
30 correlation between benthic $\delta^{18}\text{O}_c$ and sea level from -0.90 to -0.92. Additionally, we estimate
31 the phase lag between the two records by measuring their correlation with different time shifts.

1 This analysis suggests a 2 ka phase lag between LR04 and the sea level stack, likely resulting
2 from the fact that deep water temperature change leads ice volume change (e.g., Sosdian and
3 Rosenthal, 2009; Elderfield et al., 2012; Shakun et al., 2015). When we apply this 2 ka lag to
4 the smoothed LR04 stack, its correlation with sea level improves to -0.94.

5 OLS linear regression between the smoothed-and-lagged LR04 benthic $\delta^{18}\text{O}_c$ stack (x) and sea
6 level in meters (h) yields the equation

$$7 \quad h = -73 x + 251 \quad (1)$$

8 (Fig. 4, black line). Using the bootstrapped PC1 samples described in Section 4.2 and Monte
9 Carlo-style sampling of smoothing windows that range from 0 – 7 kyr and lags from 0 – 3 kyr,
10 we find that the 95% CI for the slope of this regression is -56 to -79 $\text{m}\%^{-1}$. The root mean
11 square error (rmse) for this model is 10.7 m (95% CI = 9-22 m), but the fit is better for the older
12 portion of the record (398-798 ka, rmse=10.2 m) than the more recent portion (0-397 ka,
13 rmse=11.2 m). In particular, the linear model estimates sea levels that are 10-20 m too high
14 during most highstands and lowstands back to MIS 10 at ~345 ka. The difference in fit before
15 and after 398 ka is somewhat dependent upon the assumed lag between benthic $\delta^{18}\text{O}$ and sea
16 level; the linear model fits the older portion of the record better in 84% of samples with a 3-ka
17 lag but only 61% of sampled regressions with no lag. The effect of a smaller lag is mainly to
18 increase the rmse of the older portion of the linear regression from a mean of 12.7 m (3-ka lag)
19 to 15.7 m (no lag).

20 A plot of sea level versus the smoothed and lagged benthic $\delta^{18}\text{O}_c$ (Figure 4b) suggests that the
21 relationship between the two is approximately quadratic

$$22 \quad h = -26 x^2 + 135 x - 163 \quad (2)$$

23 from 0 – 397 ka (rmse = 9.4 m, 95% CI = 8-22 m) and linear from 398-798 ka. This transition
24 appears to take place between 360-400 ka because MIS 11 clearly falls on the linear trend
25 whereas MIS 10 is much better fit by the quadratic (Figure 4a). Because this transition occurs
26 after MIS 11, the extreme duration or warmth of this interglacial might have played an
27 important role in the transition.

28 A change in the relationship between benthic $\delta^{18}\text{O}_c$ and sea level could be caused by a change
29 in the mean isotopic content of ice sheets or the relationship between ice volume and deep water
30 temperature (possibly also global surface temperature). Interglacials after MIS 11 were likely
31 warmer or had more depleted $\delta^{18}\text{O}_{\text{sw}}$ relative to ice volume. Similarly, glacial maxima were

1 probably warmer and/or had less $\delta^{18}\text{O}_{\text{sw}}$ change. Combined changes in temperature and isotopic
2 fractionation may be the most likely explanation since warmer ice sheets also probably have
3 less depleted $\delta^{18}\text{O}_{\text{ice}}$. In fact Antarctic ice cores are isotopically less depleted during MIS 5e
4 and MIS 9 than MIS 11 (Jouzel et al., 2010). Additionally, Antarctic surface temperatures and
5 CO_2 levels were similar for all three interglacials (Masson-Delmotte et al., 2010; Petit et al.,
6 1999) despite the smaller ice volume during MIS 11.

7 There is little direct evidence to explain the changing relationship between $\delta^{18}\text{O}_c$ and sea level
8 during glacial maxima because glacial values for both deep water temperature and the isotopic
9 composition of Antarctic ice are similar throughout the last 800 ka (Elderfield et al., 2012;
10 Masson-Delmotte et al., 2010). The change in glacial maxima after 400 ka could be caused by
11 less depleted $\delta^{18}\text{O}_{\text{ice}}$ in Northern Hemisphere (NH) ice sheets. Although no long records of NH
12 $\delta^{18}\text{O}_{\text{ice}}$ exist, global mean SST was 0.5-1°C warmer during MIS 2, 6, and 8 than during MIS 12
13 (Shakun et al., 2015). Alternatively, the apparent linear trend between sea level and $\delta^{18}\text{O}_c$ during
14 glacial maxima before 400 ka (Figure 4c) could be an artifact of poor sea level estimates for
15 MIS 12 and 16, which may be biased 10-20 m too high (Table 3) by missing data during
16 sapropel intervals in the Mediterranean RSL record (Rohling et al., 2014).

17 In conclusion, a systematic relationship can be defined between Late Pleistocene benthic $\delta^{18}\text{O}_c$
18 and sea level, and the functional form of this relationship likely changed after MIS 11. Change
19 in the $\delta^{18}\text{O}_c$ -sea level relationship during interglacials likely results from warmer high latitudes
20 with less depleted $\delta^{18}\text{O}_{\text{ice}}$ after 400 ka. Glacial maxima after 400 ka may also have been warmer
21 with less depleted NH $\delta^{18}\text{O}_{\text{ice}}$, but this apparent change during glacial maxima could be an
22 artifact of bias in the sea level stack during MIS 12 and 16. Changes in the relationship between
23 benthic $\delta^{18}\text{O}_c$ and sea level are also likely to have occurred during the early or mid-Pleistocene.
24 For example, the same regression probably would not apply to the 41-ka glacial cycles of the
25 early Pleistocene (Tian et al., 2003).

26 **7 Differences between sea level proxies**

27 Whereas PC1 tells us about the common variance between the sea level proxies, PC2 and PC3
28 tell us about their differences. PC2 represents 6% and 8% of the variance for the short and long
29 time windows, respectively. The scores and loads are similar for both analyses (Fig. 5 and Table
30 1) except for a sign change; therefore, we multiply by -1 the scores and loads of PC2 and PC3
31 of the short time window. Large PC2 loadings with opposite sign contributions for the 1123

1 and 607 benthic $\delta^{18}\text{O}_{\text{sw}}$ records suggest that PC2 represents differences in the $\delta^{18}\text{O}_{\text{sw}}$ of deep
2 water in the Atlantic and Pacific basins. Most notably, PC2 has a strong peak at approximately
3 250 ka (Fig. 5), associated with very low values in the 607 benthic $\delta^{18}\text{O}_{\text{sw}}$ record and very high
4 values in the 1123 benthic $\delta^{18}\text{O}_{\text{sw}}$ record (Fig. 1).

5 PC3 captures 5% of the variance in the 430-ka stack and 6% of the variance in the 798-ka stack.
6 Unlike PC1 and PC2, the loads vary between the short and long PC3 (Table 1); here we focus
7 on the short version because it contains more proxy records. In the 430-ka stack, PC3 is most
8 highly represented by the planktonic $\delta^{18}\text{O}_{\text{sw}}$ stack with a load of -0.7 and the 1123 and 607
9 benthic $\delta^{18}\text{O}_{\text{sw}}$ records with loads of about 0.5. These loads suggest that PC3 dominantly reflects
10 planktonic versus benthic differences in $\delta^{18}\text{O}_{\text{sw}}$. PC3 scores exhibit a linear trend from 0-430
11 ka, which supports the findings of previous studies that suggest planktonic $\delta^{18}\text{O}_{\text{sw}}$ should be
12 detrended for conversion to sea level (Lea et al., 2002; Shakun et al., 2015). Furthermore, PC3
13 suggests that benthic $\delta^{18}\text{O}_{\text{sw}}$ may also need to be detrended in the opposite direction. This effect
14 could be caused by long-term changes in the hydrologic cycle or deep water formation
15 processes, which lead to a change in the partitioning of oxygen isotopes between the surface
16 and deep ocean.

17 **8 Conclusions**

18 PCA indicates a strong common sea level signal in the seven records analyzed for 0-430 ka and
19 five records for 0-798 ka. Furthermore, the similarity between the short and long stacks indicate
20 that the longer stack with five records is nearly as good an approximation of sea level as the
21 seven-record stack. Sea level estimates for each interglacial vary greatly between records,
22 producing standard deviations of 11-26 m. Generally, the mean for each individual highstand
23 is greater in magnitude than our stack estimate. Based on comparison with GIA-corrected coral
24 sea level estimates for MIS 5e and 11, the stack likely reflects mean sea level for each
25 interglacial and fails to capture brief sea level highstands, such as those lasting only ~2 ka
26 during MIS 5e (Kopp et al., 2013).

27 A comparison of individual records shows that high and lowstand estimates have a mean
28 standard deviation of 17 m (for MIS 5e - 19). Uncertainty in the stack is estimated using
29 bootstrapping and random sampling, which yields a mean standard deviation for scaled PC1 of
30 9.4 m with seven records (0-430 ka) and 12 m with five records (0-798 ka). The bootstrap

1 uncertainty estimates also include age uncertainty; however, this systematically smooths the
2 bootstrap results and, thus, underestimates individual highstands relative to both individual
3 records and scaled PC1 (Figure 2c).

4 We estimate that sea level change accounts for only about 45% of the orbital-band variance in
5 benthic $\delta^{18}\text{O}_c$, compared to 65% of the LGM-to-Holocene benthic $\delta^{18}\text{O}_c$ change. Nonetheless,
6 benthic $\delta^{18}\text{O}_c$ is strongly correlated with sea level ($r = -0.9$). If LR04 benthic $\delta^{18}\text{O}_c$ stack is
7 smoothed and lagged by 2 ka, the relationship between benthic $\delta^{18}\text{O}_c$ and sea level is well-
8 described by a linear function from 398-798 ka and a quadratic function from 0-398 ka. In
9 particular, interglacials MIS 9 and 5e which had larger ice sheets than MIS 11 appear to have
10 been as warm (or warmer) than MIS 11 with isotopically less depleted ice sheets.

11 The second and third principal components of the sea level records describe differences
12 between the proxies. PC2 represents the difference between the $\delta^{18}\text{O}_{\text{sw}}$ of deep water in the
13 Atlantic and Pacific basins; a peak in PC2 scores at 250 ka indicates large differences between
14 the basins at this time. PC3 represents the differences between planktonic and benthic $\delta^{18}\text{O}_{\text{sw}}$
15 records and suggests a linear trend between the two from 0-430 ka. Thus, $\delta^{18}\text{O}_{\text{sw}}$ records vary
16 across ocean basins and between the surface and the deep. In conclusion, the stack of sea level
17 proxies presented here should be a more accurate eustatic sea level record than any of the
18 individual records it contains.

19

20

21 **Data availability**

22 The sea level stack is archived in the Supporting Information and (upon publication) at the
23 World Data Center for Paleoclimatology operated by the National Climatic Data Center of the
24 National Oceanographic and Atmospheric Association.

25 **Acknowledgements**

26 We thank all researchers who made their data available. Additionally, we thank David Lea,
27 Jeremy Shakun, Alex Simms, Charles Jones, and Leila Carvalho for beneficial discussions.

1

2 **References**

- 3 Abe-Ouchi, A., Saito, F., Kawamura, K., Raymo, M. E., Okuno, J., Takahashi, K., & Blatter,
4 H.: Insolation-driven 100,000-year glacial cycles and hysteresis of ice-sheet volume.,*Nature*,
5 *500*,7461, 190–3, [doi: 10.1038/nature12374](https://doi.org/10.1038/nature12374), 2013.
- 6 Adkins J. F., McIntyre, K., Schrag, D. P.: The Salinity, Temperature, and $\delta^{18}\text{O}$ of the Glacial
7 Deep Ocean, *Science*, 29, 298, 5599, 1769-1773, doi: 10.1126/science.1076252, 2002.
- 8 Andersen, M.B., Stirling, C.H., Potter, E.K., Halliday, A.N., Blake, S.G., Mc-Culloch, M.T.,
9 Ayling, B.F. and O'Leary, M.: High-precision U-series measurements of more than 500,000
10 year old fossil corals, *Earth and Planetary Science Letters*, 265, 229-245, 2008.
- 11 Bard, E., Hamelin, B., Fairbanks, R. G., Zindler, A.: Calibration of the ^{14}C timescale over the
12 past 30,000 years using mass spectrometric U–Th ages from Barbados corals, *Nature*, 345,
13 405-410, 1990.
- 14 Bard, E., Hamelin, B., Arnold, M., Montaggioni, L., Cabioch, G., Faure, G., & Rougerie, F. :
15 Deglacial sea-level record from Tahiti corals and the timing of global meltwater discharge,
16 *Nature*, [doi: 10.1038/382241a0](https://doi.org/10.1038/382241a0), 1996.
- 17 Bates, S. L., Siddall, M., Waelbroeck, C.: Hydrographic variations in deep ocean temperature
18 over the mid-Pleistocene transition, *Quaternary Science Reviews*, **88**, 147-158,
19 [doi:10.1016/j.quascirev.2014.01.020](https://doi.org/10.1016/j.quascirev.2014.01.020), 2014.
- 20 Bintanja, R., Roderik, S.W., van de Wal, O. J.: Modeled atmospheric temperatures and global
21 sea levels over the past million years, *Nature*, 437, 125-128 doi:10.1038/nature03975, 2005.
- 22 Blanchon, P., Eisenhauer, A., Fietzke, J., & Liebtrau, V.: Rapid sea-level rise and reef back-
23 stepping at the close of the last interglacial highstand, *Nature*, 458, 7240, 881–884, [doi:](https://doi.org/10.1038/nature07933)
24 [10.1038/nature07933](https://doi.org/10.1038/nature07933), 2009.
- 25 Boak, E. H., Turner, I. L.: Shoreline Definition and Detection: A Review, *Journal of Coastal*
26 *Research*, 214, 688–703, [doi: 10.2112/03-0071.1](https://doi.org/10.2112/03-0071.1), 2005.

- 1 Bowen, D. Q. Sea level, ~400,000 years ago (MIS 11): analogue for present and future sea-
2 level?, *Clim. Past*, 6, 19–29, 2010.
- 3 Bryden, H. L., Kinder T.H.: Steady two-layer exchange through the Strait of Gibraltar, *Deep*
4 *Sea Res.*, 38, S1, S445–S463, 1991.
- 5 Clark, P.U., Dyke, A.S., Shakun, J.D., Carlson, A.E., Clark, J., Wohlfarth B., Mitrovica, J. X.,
6 Hostetler S.W., McCabe A. M.: The Last Glacial Maximum, *Science*, 325, 5941, 710-714,
7 doi: 10.1126/science.1172873, 2009.
- 8 Clark, P. U., et al.: Global climate evolution during the last deglaciation, *Proceedings of the*
9 *National Academy of Sciences*, 109, 19, E1134–E1142, doi: [10.1073/pnas.1116619109](https://doi.org/10.1073/pnas.1116619109), 2012.
- 10 Creveling, J.R., Mitrovica, J.X., Hay, C.C., Austermann, J., Kopp, R.E.: Revisiting tectonic
11 corrections applied to Pleistocene sea-level highstands, *Quat. Sci. Rev.*, 111, 72-80,
12 doi:[10.1016/j.quascirev.2015.01.003](https://doi.org/10.1016/j.quascirev.2015.01.003), 2015.
- 13 Duplessy, J.C., Labeyrie, L., Waelbroeck, C.: Constraints on the ocean isotopic enrichment
14 between the Last Glacial Maximum and the Holocene: Paleoceanographic implications, *Quat.*
15 *Sci. Rev.*, 21, 315-330, 2002.
- 16 Dutton, A, Carlson, A., Long, A., Milne, G., Clark, P., DeConto, R., Horton, B. P., Rahmstorf
17 S., Raymo, M.: Sea-level rise due to polar ice-sheet mass loss during past warm periods,
18 *Science*, 349, 6244, 153 aaa4019–1. <http://doi.org/10.1126/science.aaa4019>, 2015.
- 19 Dutton, A., Lambeck, K.: Ice Volume and Sea Level During the Last Interglacial, *Science*,
20 337, 216–220, 2012.
- 21 Dwyer, G. S., Cronin, T. M., Baker, P. A., Raymo, M. E., Buzas, J. S., & Corrige, T.: North
22 Atlantic Deepwater Temperature Change During Late Pliocene and Late Quaternary Climatic
23 Cycles, *Science*, 270, 1347–1351, doi: [10.1126/science.270.5240.1347](https://doi.org/10.1126/science.270.5240.1347), 1995.
- 24 Edwards, R.L., Beck, J. W., Burr, G. S., Donahue, D. J., Chappell, J. M. A., Bloom, A. L.,
25 Druffel, E. R. M., Taylor, F. W.: A Large Drop in Atmospheric $^{14}\text{C}/^{12}\text{C}$ and Reduced Melting
26 in the Younger Dryas, Documented with ^{230}Th Ages of Corals, *Science*, 260, 962-968, 1993.

1 Elderfield, H., Ferretti, P., Greaves, M., Crowhurst, S. J., McCave, I.N., Hodell, D. A.,
2 Piotrowski, A. M.: Evolution of ocean temperature and ice volume through the Mid-
3 Pleistocene Climate Transition, *Science*, 337,6095, 704-709, doi:10.1126/science.1221294,
4 2012.

5 Fairbanks, R.G. : A 17,000 year glacio-eustatic sea level record: influence of glacial melting
6 rates on the Younger Dryas event and deep-ocean circulation, *Nature*, 342, 637-642, 1989.

7 Ganopolski, A., Calov, R.: The Role of Orbital Forcing, Carbon Dioxide and Regolith in 100
8 kyr Glacial Cycles, *Climate of the Past*, 7, 1415-1425, 2011.

9 Gibbons, F. T., Oppo, D. W., Mohtadi, M., Rosenthal, Y., Cheng, J., Liu, Z., Linsley, B.K.:
10 Deglacial $\delta^{18}\text{O}$ and hydrologic variability in the tropical Pacific and Indian Oceans, *Earth and*
11 *Planetary Science Letters*, 387, 240–251, 2014.

12 Govin, A., Braconnot, P., Capron, E., Cortijo, E., Duplessy, J.-C., Jansen, E., Labeyrie, L.,
13 Landais, A., Marti, O., Michel, E., Mosquet, E., Risebrobakken, B., Swingedouw, D.,
14 Waelbroeck, C., Persistent influence of ice sheet melting on high northern latitude climate
15 during the early Last Interglacial, *Climate of the Past*, 8, 2, 483–507, doi: 10.5194/cp-8-483-
16 2012, 2012.

17 Grant, K.M., Rohling, E.J., Bronk Ramsey, C., Cheng, H., Edwards, R.L., Florindo, F.,
18 Heslop, D., Marra, F., Roberts, A.P. Tamisiea, M.E., and Williams, F.: Sea-level variability
19 over five glacial cycles, *Nature Communications*, 5, 5076, doi: 10.1038/ncomms6076, 2014.

20 Hanebuth, T., Stattegger, K., Grootes, P. M.: Rapid Flooding of the Sunda Shelf: A Late-
21 Glacial Sea-Level Record, *Science*, 288,1033–1035, doi: [10.1126/science.288.5468.1033](https://doi.org/10.1126/science.288.5468.1033),
22 2000.

23 Hay, C., Mitrovica, J. X., Gomez, N., Creveling, J. R., Austermann, J., & E. Kopp, R.: The
24 sea-level fingerprints of ice-sheet collapse during interglacial periods, *Quaternary Science*
25 *Reviews*, 87, 60–69, doi: [10.1016/j.quascirev.2013.12.022](https://doi.org/10.1016/j.quascirev.2013.12.022), 2014.

26 Horton, B. P.: Late Quaternary Relative Sea-level Changes in Late Quaternary Relative Sea-
27 level Changes in Mid-latitudes, *Encyclopedia of Quaternary Science*, 2064–3071, 2006.

- 1 Huybers, P. and C. Wunsch: A depth-derived Pleistocene age model: Uncertainty estimates,
2 sedimentation variability, and nonlinear climate change, *Paleoceanography*, 19, 1–24, [doi:](https://doi.org/10.1029/2002PA000857)
3 [10.1029/2002PA000857](https://doi.org/10.1029/2002PA000857), 2004.
- 4 Jouzel, J., Masson-Delmotte, V., Cattani, O., Dreyfus, G. Falourd, S., Hoffmann, G., Minster,
5 B., Nouet, J., Barnola, J. M., Chappellaz, J., Fischer, H., Gallet, J. C., Johnsen, S.,
6 Leuenberger, M., Loulergue, L., Luethi, D., Oerter, H., Parrenin, F., Raisbeck, G., Raynaud,
7 D., Schilt, A., Schwander, A., Selmo, E., Souchez, R., Spahni, R., Stauffer, B., Steffensen, J.
8 P. Stenni, B., Stocker, T. F., Tison, J. L., Werner, M., Wolff, E. W.: Orbital and Millennial
9 Antarctic Climate Variability over the Past 800,000 Years, *Science* 317, 793, doi:
10 [10.1126/science.1141038](https://doi.org/10.1126/science.1141038), 2007.
- 11 Kopp, R. E., Simons, F. J., Mitrovica, J. X., Maloof, A. C., Oppenheimer M.: Probabilistic
12 assessment of sea level during the last interglacial stage, *Nature*, 462, 863-867,
13 doi:10.1038/nature08686, 2009.
- 14 Kopp, R. E., Simons, F. J., Mitrovica, J. X., Maloof, A. C., Oppenheimer M.: A probabilistic assessment of sea
15 level variations within the last interglacial stage, *Geophys. J. Int.*, 193, 711–716, 2013. Lambeck, K., Esat, T.
16 M., & Potter, E.-K. (2002). Links between climate and sea levels for the past three million
17 years, *Nature*, 419, 6903, 199–206, [doi: 10.1038/nature01089](https://doi.org/10.1038/nature01089), 2002.
- 18 Lambeck, K., Rouby, H., Purcell A., Sun, Y., Sambridge, M.: Sea level and global ice
19 volumes from the Last Glacial Maximum to the Holocene, *Proc. Nat. Ac. Sci.*, 111, 43,
20 doi:10.1073/pnas.1411762111, 2014.
- 21 Lea, D. W., Martin, P. a., Pak, D. K., & Spero, H. J.: Reconstructing a 350 ky history of sea
22 level using planktonic Mg/Ca and oxygen isotope records from a Cocos Ridge core,
23 *Quaternary Science Reviews*, 21,1-3, 283–293, doi: 10.1016/S0277-3791(01)00081-6, 2002.
- 24 Lisiecki, L. E., Raymo, M. E.: A Pliocene-Pleistocene stack of 57 globally distributed benthic
25 $\delta^{18}\text{O}$ records, *Paleoceanography*, 20, PA1003, doi:10.1029/2004PA001071, 2005.
- 26 Lisiecki, L. E., & Raymo, M. E. : Diachronous benthic $\delta^{18}\text{O}$ responses during late
27 Pleistocene terminations, *Paleoceanography*, 24, 3, [doi: 10.1029/2009PA001732](https://doi.org/10.1029/2009PA001732). 2009.
- 28 Masson-Delmotte, V., Stenni, B., Jouzel, J., Landais, A., Röthlisberger R., Minster B.,

- 1 Hansen, J., Pol K., Barnola, J.M., Mikolajewicz, U., Braconnot, P., Chappellaz, J., Otto-
2 Bliesner, B., Cattani, O., Krinner, G.: EPICA Dome C record of glacial and interglacial
3 intensities, *Quat. Sci. Rev.*, 29, 113-128, 2010.
- 4 Medina-Elizalde, M.: A compilation of coral sea level benchmarks: Implications and new
5 challenges, *Earth. Planet. Sc. Lett.*, 362, 310-318, 2013.
- 6 Petit, J. R., Jouzel, J., Raynaud, D., Barkov, N. I., Barnola, J. -M., Basile, I., Bender, M.,
7 Chappellaz, J., Davisk, M., Delaygue, G., Delmotte, M., Kotlyakov, V. M., Legrand, M.,
8 Lipenkov, V. Y., Lorius, C., Pépin, L., Ritz, C., Saltzman, E., Stievenard M.: Climate and
9 atmospheric history of the past 420,000 years from the Vostok ice core, Antarctica, *Nature*,
10 399, 429-436, 1999.
- 11 Martin, P. A., Lea, D. W., Rosenthal, Y., Shackleton, N. J., Sarnthein, M., & Papenfuss, T.:
12 Quaternary deep sea temperature histories derived from benthic foraminiferal Mg/Ca, *Earth
13 and Planetary Science Letters*, 198,1-2, 193–209. [doi: 10.1016/S0012-821X\(02\)00472-7](https://doi.org/10.1016/S0012-821X(02)00472-7),
14 2002.
- 15 Medina-Elizalde, M.: A global compilation of coral sea-level benchmarks: Implications and
16 new challenges, *Earth and Planetary Science Letters*, 362, 310–318, [doi:](https://doi.org/10.1016/j.epsl.2012.12.001)
17 [10.1016/j.epsl.2012.12.001](https://doi.org/10.1016/j.epsl.2012.12.001). 2013.
- 18 Muhs, D. R., Meco, J., Simmons, K. R. : Uranium-series ages of corals, sea level history, and
19 palaeozoogeography, Canary Islands, Spain: An exploratory study for two Quaternary
20 interglacial periods, *Palaeogeography, Palaeoclimatology, Palaeoecology*, 394, 99–118, [doi:](https://doi.org/10.1016/j.palaeo.2013.11.015)
21 [10.1016/j.palaeo.2013.11.015](https://doi.org/10.1016/j.palaeo.2013.11.015), 2014.
- 22 Raymo, M. E., Mitrovica, J. X.: Collapse of polar ice sheets during the stage 11 interglacial,
23 *Nature*, [doi:10.1038/nature10891](https://doi.org/10.1038/nature10891), 2012.
- 24 Raymo M.E., Ruddiman W.F., Shackleton N.J., Oppo D.W.: Evolution of Atlantic-Pacific
25 $\delta^{13}\text{C}$ gradients over the last 2.5 m.y., *Earth Planet. Sci. Lett.*, 97, 353-368, 1990.
- 26 Rohling, E.J., Grant, K., Bolshaw, M., Roberts, A.P., Siddall, M., Hemleben, C., Kucera, M.:
27 Antarctic temperature and global sea level closely coupled over the past five glacial cycles.
28 *Nat. Geosci.*, 2, 500–504, 2009.

- 1 Rohling, E. J. *et al.* Reconstructing past planktic foraminiferal habitats using stable isotope
2 data: a case history for Mediterranean sapropel S5, *Mar. Micropaleontol.* 50, 89–123, 2004.
- 3 Rohling, E. J., Grant, K.M., Bolshaw, M., Roberts, A. P., Siddall, M., Hemleben C. Kucera,
4 M., Foster, G.L., Marino, G., Roberts, A.P., Tamsiea, M.E., and Williams, F.: Sea-level and
5 deep-sea-temperature variability over the past 5.3 million years, *Nature*, 508, 477–482, 2014.
- 6 Schiebel, R., Zeltner, A., Treppke, U. F., Waniek, J.J., Bollmann, J., Rixen, T., Hemleben, C.:
7 Distribution of diatoms, coccolithophores and planktic foraminifera in the Arabian Sea, *Mar.*
8 *Micropaleontol.*, 51, 345-371, doi:10.1016/j.marmicro.2004.02.001, 2004.
- 9 Shackleton, N. J.: Attainment of isotopic equilibrium between ocean water and the
10 benthonic foraminifera genus *Uvigerina*: Isotopic changes in the ocean during the last glacial,
11 *Colloque International sur les Methodes Quantitatives d'Etude des Variation du*
12 *Climat au Sours du Pleistocene*, Coll. Int. C.N.R.S., 219, 203–209, 1974.
- 13 Shakun, J.D., Clark, P.U., He, F., Marcott, S. A., Mix, A. C., Liu, Z., Otto-Bliesner, B.,
14 Schmittner A., Bard E.: Global warming preceded by increasing carbon dioxide
15 concentrations during the last deglaciation, *Nature*, 484, 49–54, doi:10.1038/nature10915,
16 2012.
- 17 Shakun, J. D., Lea, D. W., Lisiecki, L. E., Raymo, M. E.: An 800-kyr record of global surface
18 ocean $\delta^{18}\text{O}$ and implications for ice volume-temperature coupling, *Earth. Planet. Sc. Lett.*,
19 426, 58–68, 2015
- 20 Siddall, M., Hönisch, B., Waelbroeck, C., Huybers, P.: Changes in deep Pacific temperature
21 during the mid-Pleistocene transition and Quaternary, *Quat. Sci. Rev.*, 29, 170-181, 2010.
- 22 Siddall, M., Smeed, D.A., Hemleben, Ch., Rohling, E.J., Schmeltzer, I., and Peltier, W.R.:
23 Understanding the Red Sea response to sea level, *Earth. Planet. Sc. Lett.*, 225, 421-434, 2004.
- 24 Skinner, L. C., Shackleton, N. J. : An Atlantic lead over Pacific deep-water change across
25 Termination I: implications for the application of the marine isotope stage stratigraphy,
26 *Quaternary Science Reviews*, 24, 5-6, 571–580, [doi: 10.1016/j.quascirev.2004.11.008](https://doi.org/10.1016/j.quascirev.2004.11.008), 2005.

1 Sostdian S., Rosenthal Y.: Deep-Sea Temperature and Ice Volume Changes Across the
2 Pliocene-Pleistocene Climate Transitions, *Science*, 17, 325, 5938, 306-310, doi:
3 10.1126/science.1169938, 2009.

4 Stein, M., Wasserburg, G. ., Aharon, P., Chen, J. ., Zhu, Z. ., Bloom, a, & Chappell, J.: TIMS
5 U-series dating and stable isotopes of the last interglacial event in Papua New Guinea,
6 *Geochimica et Cosmochimica Acta*, 57, 11, 2541–2554, doi: 10.1016/0016-7037(93)90416-T,
7 1993.

8 Stern, J. V., Lisiecki, L.E.: Termination 1 timing in radiocarbon dated regional benthic $\delta^{18}\text{O}$
9 stacks, *Paleoceanography*, 29, 1127-1142, doi:10.1002/2014PA002700, 2014.

10 Stirling, C. H., Esat, T. M., McCulloch, M. T., & Lambeck, K. (1995): High-precision U-
11 series dating of corals from Western Australia and implications for the timing and duration of
12 the Last Interglacial, *Earth and Planetary Science Letters*, 135, 1-4, 115–130 [doi:](https://doi.org/10.1016/0012-821X(95)00152-3)
13 [10.1016/0012-821X\(95\)00152-3](https://doi.org/10.1016/0012-821X(95)00152-3), 1995.

14 Thompson, W. G., Goldstein, S. L.: Open-System Coral Ages Reveal Persistent Suborbital
15 Sea-Level Cycles, *Science*, 308, 5720, 401-404, doi: 10.1126/science.1104035, 2005.

16 Tian, L., Yao T., Schuster, P.F., White, J.W.C., Ichiyanagi K., Pendall, E., Pu, J., Yu W.:
17 Oxygen-18 concentrations in recent precipitation and ice cores on the Tibetan Plateau, *J.*
18 *Geophys. Res.*, 108, 4293, D9, 2003. Waelbroeck, C., Labeyrie, L., Michel, E., Duplessy J.C.,
19 McManus J.: Sea-level and deep water temperature changes derived from benthic
20 foraminifera isotopic records, *Quaternary Sci. Rev.*, 21, 295–305, 2002.

21 Wang, P., Tian, J. & Lourens, L. J.: Obscuring of long eccentricity cyclicity in Pleistocene
22 oceanic carbon isotope records, *Earth Planet. Sci. Lett.*, 290, 319–330 , 2010.

23

1 Table 1. Principal Component Analysis (PCA) loading for each proxy record. “Short” refers to
 2 the 0-430 ka time window, and “Long” refers to 0-798 ka. Numbers in parentheses give the
 3 percent variance explained by each principal component.

4

	PC1 Short (83%)	PC1 Long (77%)	PC2 Short (6%)	PC2 Long (8%)	PC3 Short (5%)	PC3 Long (6%)
Inverse model (Bintanja et al., 2005)	0.4	0.48	-0.05	-0.11	-0.16	0.02
Pac. benthic $\delta^{18}\text{O}_{\text{sw}}$ (Elderfield et al., 2012)	0.34	0.44	-0.7	-0.5	0.52	0.67
Planktonic $\delta^{18}\text{O}_{\text{sw}}$ (Shakun et al., 2015)	0.37	0.45	-0.01	-0.19	-0.65	-0.65
RSL_{Med} (Rohling et al, 2014)	0.38	0.45	0	0.01	0.04	-0.27
Atl. benthic $\delta^{18}\text{O}_{\text{sw}}$ (Sosdian and Rosenthal, 2009)	0.35	0.42	0.7	0.84	0.51	0.26
$\delta^{18}\text{O}_c$ regression (Waelbroeck et al., 2002)	0.4	-	0.08	-	-0.11	--
RSL_{Red} (Rohling et al., 2009)	0.4	-	-0.01	-	-0.07	--

5

6

7

1 Table 2. Sea level highstand and lowstand estimates from individual records (in meters above
 2 modern). See Table 1 for references. The last column gives the mean values from nine cores in
 3 Bates et al (2014); these estimates were not included in our PCA.

Marine Isotope Stage	Age (ka)	Inverse model	Pac. benthic $\delta^{18}\text{O}_{\text{sw}}$	RSL Red	RSL Med	Plank. $\delta^{18}\text{O}_{\text{sw}}$	Atl. benthic $\delta^{18}\text{O}_{\text{sw}}$	$\delta^{18}\text{O}_c$ regression	Bates et al. (2014) mean
2	18-25	-123	-113	-114	-120	-130	-124	-123	-133
5e	119-126	0	3	18	-4	-10	28	4.9	12
6	135-141	-123	-130	-99	-94	-138	-97	-129	-130
7a-c	197-214	-20	12	14	12	-16	34	-3.6	-3
7e	236-255	-18	16	-3	1	-20	-6.2	-9.4	-10
9	315-331	-0.5	40	11	-5	-27	43	5	8
10	342-353	-111	-96	-114	-77	-98	-112	-126	-122
11	399-408	0	58	4	12	-5	57	5.7	9
12	427-458	-126	-146	-118		-142	-100		-147
13	486-502	-29	18		-8	-11	32		-5
16	625-636	-126	-113			-144	-125		-141
17	682-697	-23	31		0.5	-12	8.1		-4
19	761-782	-21	21		7.2	-1	-6.8		-2

4

5

6

7

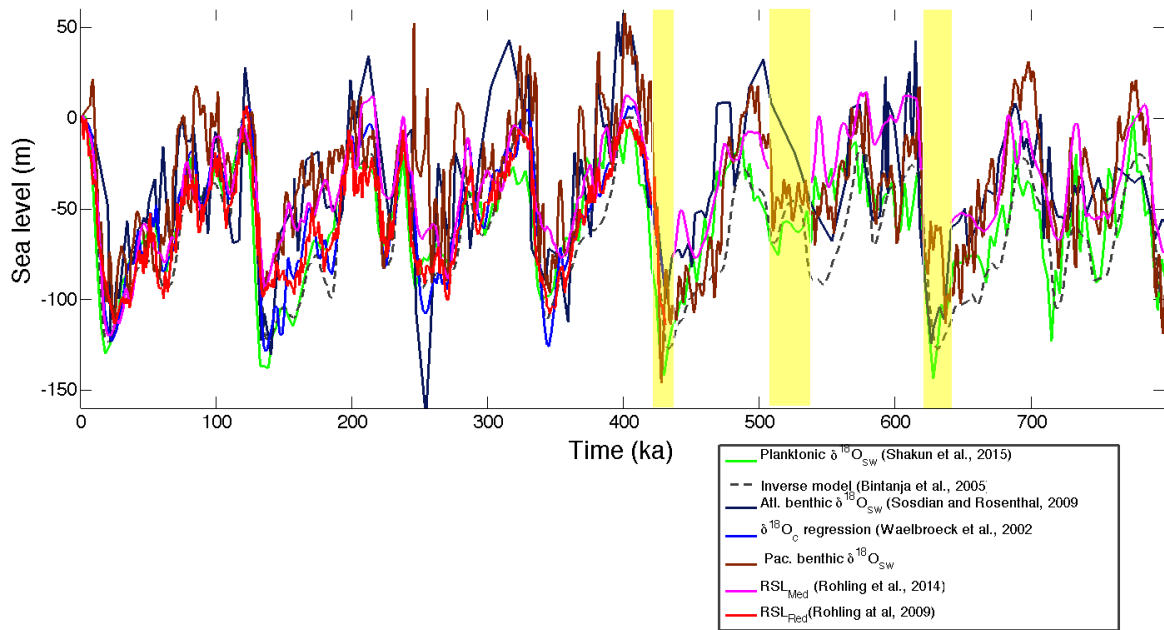
1 Table 3. Mean and standard deviation of sea level highstand and lowstand estimates (in meters
 2 above modern) from Table 2 compared to scaled PC1 and GIA-corrected from corals and other
 3 coastal proxies. GIA-corrected estimates for MIS 2 are from Clark et al. (2009) and Lambeck
 4 et al. (2014), for MIS 5e from Dutton et al. (2015), and for MIS 11 from Raymo and Mitrovica
 5 (2013). Bootstrap 95% confidence intervals are from sampling the seven-record short PC1 for
 6 MIS 2 – 11 and from the five-record long PC1 for MIS 12 – 19.

Marine Isotope Stage	Age Range (ka)	Standard deviation	Mean	GIA corrected estimates	Scaled PC1 (0-430 ka)	Scaled PC1 (0-798 ka)	Bootstrap 95% confidence interval
2	18-25	7	-123	-130 to -134	-130	-130	-136 to -128
5e	119-126	12	7	6 to 9	3	-1	-14 to 17
6	135-141	18	-118		-123	-125	-142 to -111
7a-c	197-214	18	4		-7	-5	-25 to 14
7e	236-255	11	-6		-9	-13	-32 to -1
9	315-331	23	9		-1	-2	-27 to 20
10	342-353	16	-107		-108	-103	-128 to -92
11	399-408	25	18	6 to 13	16	19	-11 to 40
12	427-458	19	-130			-124	-163 to -100
13	486-502	22	-1			-11	-35 to 16
16	625-636	13	-130			-115	-149 to -87
17	682-697	19	0			-9	-28 to 15
19	761-782	14	0			-6	-25 to 10

7

8

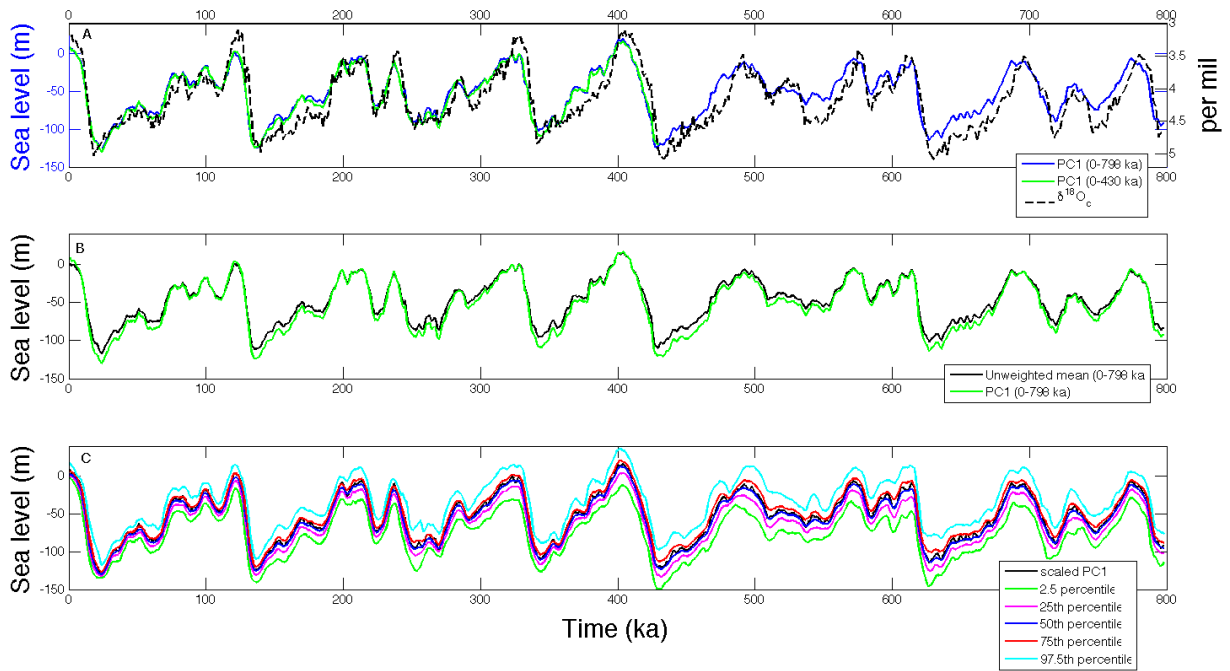
1



2

3 Figure 1. Eustatic and relative sea level estimates for the seven records on the LR04 age model
4 (Lisiecki and Raymo, 2004). Yellow bars mark the sapropel layers removed from the
5 Mediterranean RSL record (Rohling et al, 2014).

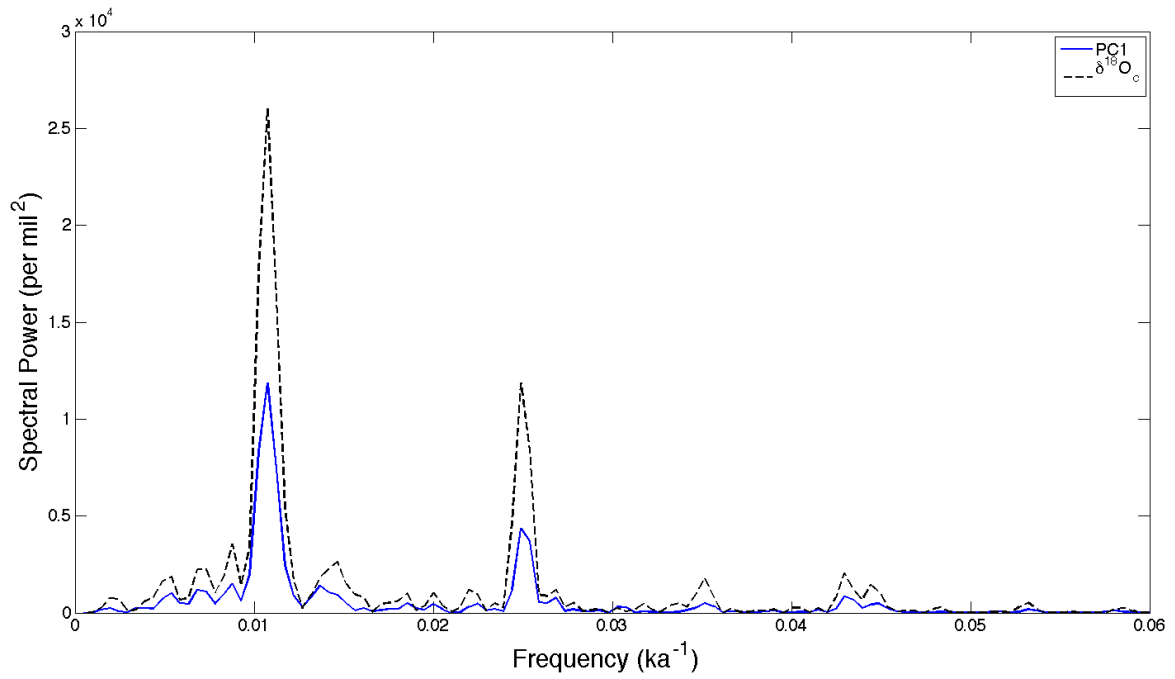
6



1
2
3
4
5
6
7

Figure 2. A. Long and short sea level stacks compared to the LR04 benthic $\delta^{18}O_e$ stack (Lisiecki and Raymo, 2005). B. Scaled PC1 compared to unweighted mean of individual records. Scaled PC1 is comprised of short PC1 (0-431 ka) pasted to long PC1 (431-798 ka). C. Scaled PC1 compared with percentile levels from the bootstrap results, which are also plotted as a composite of the short (0-431 ka) and long (431-798 ka) time windows.

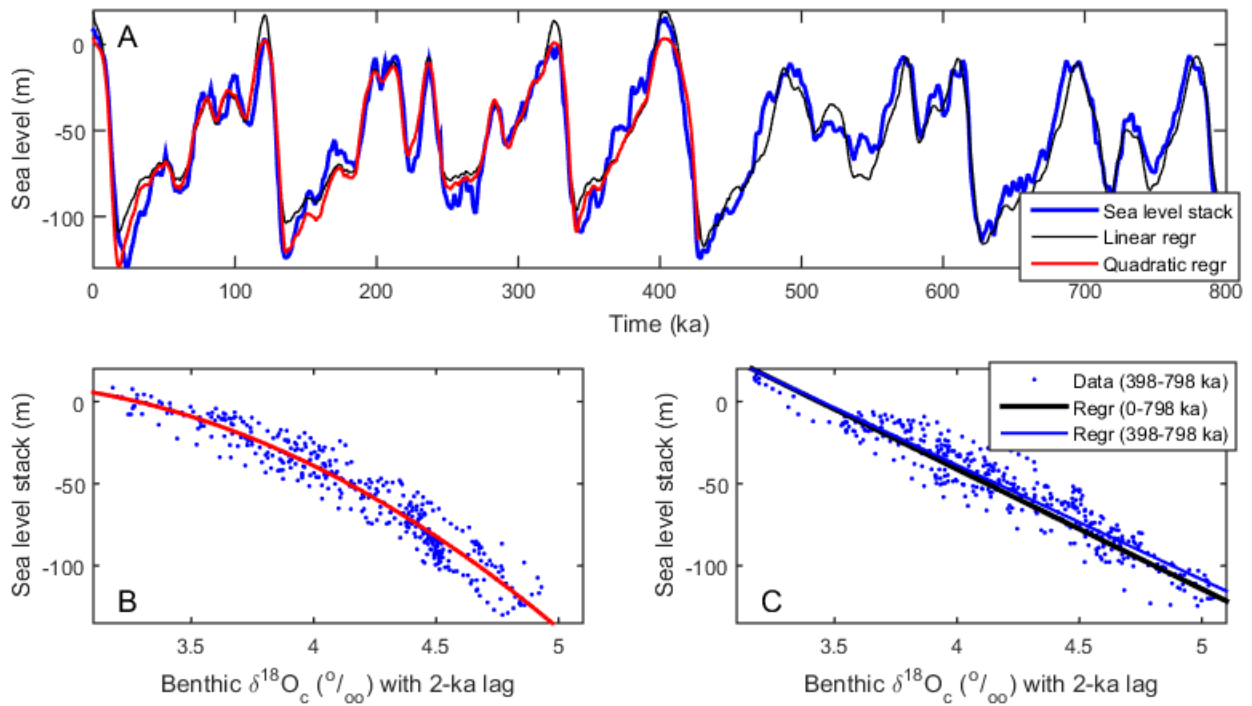
1



2

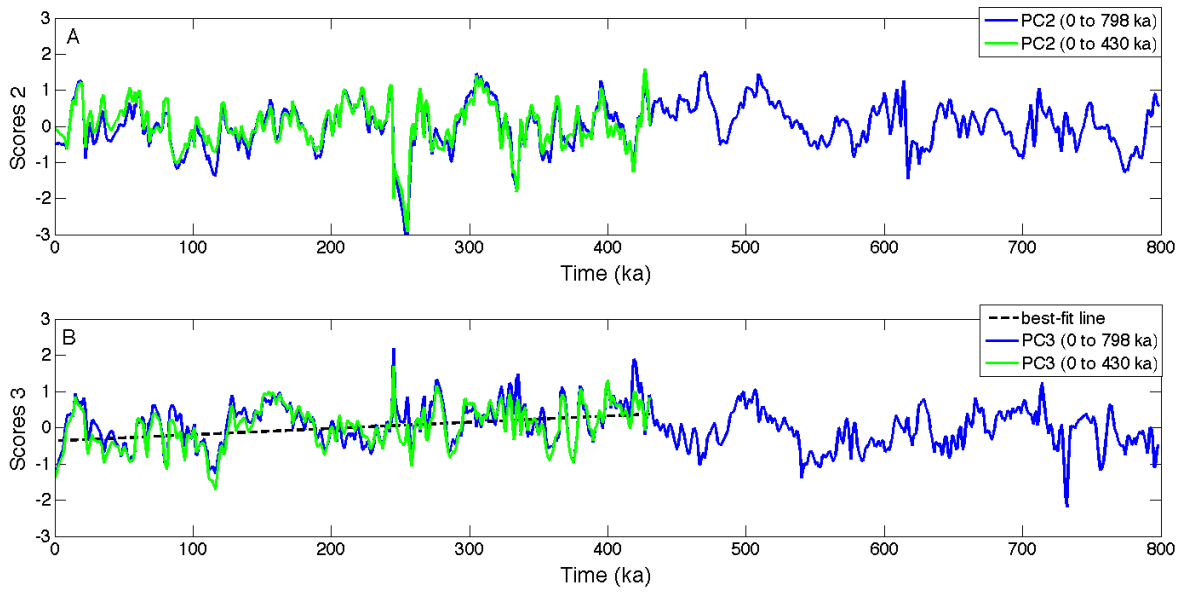
3 Figure 3. Spectral analysis for composite sea level stack (scaled PC1) converted to its $\delta^{18}O_{sw}$
4 contribution using 0.009‰m^{-1} and benthic $\delta^{18}O_c$ stack (Lisiecki and Raymo, 2005) from 0-798
5 ka.

6



1
2
3
4
5
6

Figure 4. Comparison of benthic $\delta^{18}\text{O}_c$ and sea level. A. Linear and quadratic sea level models (Eq. 1 and 2, respectively) using smoothed benthic $\delta^{18}\text{O}_c$ (Lisiecki and Raymo, 2005) lagged by 2 ka. B. Data from 0-397 ka with quadratic regression (red line). C. Data from 398-798 ka with linear regression for 0-798 ka (black line) and 398-798 ka (blue line).



1

2 Figure 5. Second and third principal components for 0-430 ka and 0-798 ka. A. Scores for PC2
 3 largely reflect difference between Atlantic and Pacific benthic $\delta^{18}\text{O}_{\text{sw}}$. B. Scores for PC3 largely
 4 reflect the difference benthic and planktonic $\delta^{18}\text{O}_{\text{sw}}$. Dashed black line marks linear trend from
 5 0-430 ka.